Available online at www.sciencedirect.com
ScienceDirect
Catalysis Today 128 (2007) 3–12
CATALYSIS TODAY
www.elsevier.com/locate/cattod

MRI strategies for characterising two-phase flow in parallel channel ceramic monoliths

Andrew J. Sederman, Jonathan J. Heras, Michael D. Mantle, Lynn F. Gladden *

University of Cambridge, Department of Chemical Engineering, Pembroke Street, Cambridge CB2 3RA, United Kingdom

Available online 8 June 2007

Abstract

Magnetic resonance (MR) techniques are now being used widely in chemical engineering research. In recognition of Mike Winterbottom's contribution to the field of ceramic monolith reactors, recent developments in the application of MR techniques to the study of two-phase flow in parallel channel ceramic monoliths are reported. Two new approaches are described, both of which can be applied to single- and two-phase flow. In particular, we report the development of a displacement tracking technique which allows temporal variations in velocity, occurring on timescales of ~10 ms, to be monitored over periods of up to 1 s. The upper limit on liquid velocity that can be measured using this approach is ~5–10 m s^{-1}. The techniques are introduced and illustrated with reference to co-current gas–liquid up-flow operation in a monolith rated at 200 channels per square inch.

Keywords: Magnetic resonance imaging; Catalysis; Hydrodynamics; Monolith reactors

1. Introduction

Magnetic resonance (MR) techniques are now becoming established alongside γ- and X-ray absorption, ultrasound attenuation, laser and phase Doppler anemometry, particle imaging velocimetry, and capacitance tomography as standard research tools for the characterisation of single- and multi-phase flows in reactor environments [1,2].

This paper addresses the development and implementation of MR methods to study single- and two-phase flow in parallel channel ceramic monoliths. Regular and irregular catalyst packings are used extensively in the chemical industry for promoting mass transfer and chemical reaction between gas and liquid. Traditionally, randomly packed beds of catalyst particles operating in co-current down-flow operation, often termed trickle-bed reactors, have been used because of the high reaction rates per unit volume achievable. More recently, structured supports are increasingly considered for use because of the potential improvements they offer with respect to, for example, the decoupling of heat and mass transfer phenomena, operation under reduced pressure drop conditions and at much higher gas/liquid flow rates, and a greater resistance to attrition [3–5]. One might also expect that the uniformity of channel structure may give improved homogeneity and predictability in performance compared to that of a fixed bed of traditional catalyst packing material which is inherently associated with significant flow heterogeneity [2]. Monoliths, which comprise a metal or ceramic structure with a large number of straight or parallel channels, are a particular example of structured supports and their use in solid-catalysed gas-phase chemical reactions is well established; e.g. the monolithic exhaust gas converter used throughout the automotive industry. In contrast, the application of monoliths to gas–liquid reactions, of particular interest in fine chemicals production, is not well advanced and a significant research activity exists to provide the necessary understanding to enable reliable scale-up for process operation [6,7]. Undoubtedly, such efforts will be aided significantly by the use of *in situ* probes of the multi-phase transport and reaction phenomena occurring within these porous structures. Imaging of gas–liquid flow in ceramic monoliths was first reported by Mewes et al. [8] using the capacitance tomography technique. While temporal resolution of capacitance tomography is high (100 images per second can be achieved), spatial resolution is relatively low with typical

* Corresponding author. Tel.: +44 1223 334762; fax: +44 1223 334796.
E-mail address: Gladden@cheng.cam.ac.uk (L.F. Gladden).

0920-5861/$ – see front matter
doi:10.1016/j.cattod.2007.04.012

Nomenclature

G	magnetic field gradient vector (T m^{-1})
k	reciprocal space vector (m^{-1})
k_i	component of the reciprocal space vector in the ith direction (m^{-1})
n_i	number of images
n_p	number of phase increments per image
n_v	number of times pulse sequence is looped; i.e. number of images acquired from a single radio-frequency excitation
r	real space vector (m)

Greek letters

Δ	the echo time in the radio-frequency pulse sequence (s)
ϕ	phase shift of the nuclear spin system (rad)
γ	gyromagnetic ratio (rad s^{-1} T^{-1})
ρ	nuclear spin density (m^{-3})

in-plane resolution being 5–10% of the diameter of the system under investigation, thereby making visualisation of phase distribution within a single channel impossible. More recently, Bauer et al. [9] have used γ-ray computed tomography to measure the time-averaged liquid distribution over monolith cross-sections. The application of an integrated optical sensor, exploiting the phenomenon of total internal reflection, has also been reported as a method for detecting the number, dimensions and velocity of individual slugs and bubbles within channels [10]. MR Imaging (or MRI) has the potential for achieving relatively high spatial resolution (say, 30–200 μm) but improvements in temporal resolution have been necessary to enable it to address dynamic processes in reactors and two-phase flows. MR techniques also offer the opportunity to image conversion *in situ*, and reports of applications to fixed-bed reactors already exist [11–14]. However, at the present time, it is MR studies of flow within reactors which have received more attention and it is the development of MR flow imaging methods to study single- and two-phase flow within ceramic monoliths which is the subject of this paper.

To date, there have been several reports of MRI studies of flow and gas–liquid distribution within parallel channel ceramic monoliths. The majority of these reports have considered two-dimensional (2D) images acquired perpendicular to the direction of flow. For example, Koptyug et al. [15,16] have reported studies of single-phase flow in monoliths. The first of these two papers reported quantitative, spatially resolved velocity maps of thermally polarized acetylene, propane, butane and water flowing through the channels of alumina monoliths; images were acquired with an in-plane spatial resolution of 400 μm [15]. The monoliths had a channel cross-section of 4.0 mm × 4.0 mm and a wall thickness of 1.0 mm. Axial gas phase velocities of up to 0.93 m s^{-1} (Re = 570) were studied. The 2D flow maps were acquired perpendicular to the superficial flow direction and showed a highly non-uniform distribution of shear rates within the individual monolith channels. Typical image acquisition times were 20–40 min. This work was extended to consider both single-phase liquid and gas flow and mass transport phenomena in two different cylindrical monolith catalysts (one with triangular channels, the other with square channels) at different axial locations within a given monolith [16].

Heibel et al. [17,18] have addressed two-phase flow in the film flow regime and reported investigations of liquid distributions in the plane perpendicular to the direction of superficial flow. In particular, these workers addressed the accumulation of liquid in the corners of the square channels of the monolith. A four-channel monolith array was used in which the preferential flow of the liquid in the corners of the channels was studied as a function of the nature of distributor and the liquid flow rate used. Non-uniformities in the liquid distribution over the four corners of the square channels were apparent in addition to any mal-distribution over the cross-section of the monolith.

The first images of two-phase flow within individual channels, studied in real-time, along the direction of superficial flow, were reported by Mantle et al. [19] as part of a collaboration with Mike Winterbottom. The work employed a novel MR pulse sequence named Single Excitation Multiple Image RARE (SEMI-RARE) [20], which is a variant of the Rapid Acquisition with Relaxation Enhancement (RARE) pulse sequence [21]. The SEMI-RARE pulse sequence acquires *multiple images* (up to ∼120) from a single radio-frequency (r.f.) excitation; i.e. not just a *single* complete image from a single excitation. The actual number of images acquired from a single excitation is determined by the characteristic nuclear spin relaxation times of the system under study. The SEMI-RARE technique allows images along the length of the monolith to be recorded with the slice thickness being smaller than the width of an individual channel; thus we can image the two-phase flow characteristics (liquid slug and gas bubble dimensions) in adjacent channels within the monolith. In our early work [19], the SEMI-RARE pulse sequence was used to image Taylor, or bubble-train, gas–liquid down-flow within the parallel channels of a ceramic monolith. Fig. 1 shows the nature of the data obtained. The experimental set-up was as follows. A Perspex® column, of 48 mm i.d., containing a cylindrical, square-channel monolith was positioned within the vertical bore of the magnet. The ceramic (cordierite) monolith of diameter 43 mm and length 0.15 m, was rated at 200 channels per square inch (cpsi) with each channel having a square cross-section of side 1.7 mm. Gas (compressed air) and liquid (water) were introduced at the top of the column as two separate feed streams with flow rates of 1 l min^{-1} (9.2 mm s^{-1}) and 6 l min^{-1} (55.3 mm s^{-1}) respectively; the superficial flow direction was along the axis of the magnet; i.e. in the z-direction. The high velocity liquid jet at the column inlet, created an intensely agitated gas–liquid dispersion [22] flowing downwards and the upper surface of the monolith was positioned at a distance 0.85 m below the inlet. In this example, each image took 160 ms to acquire and the time between the start of successive acquisitions was also 160 ms. Therefore, effective image times are taken as 80, 240, 400 and 560 ms after the initial excitation.

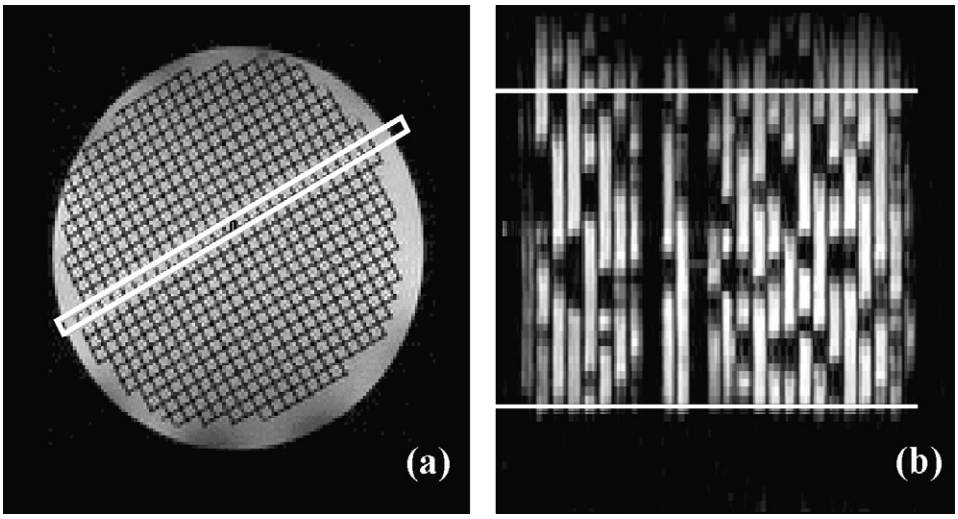

Fig. 1. SEMI-RARE MR images of a parallel channel ceramic monolith. An *xy*-image of the fully water-saturated monolith (a) shows the internal structure of the monolith; each channel has a side length 1.7 mm. The highlighted region shows the position of the image slice in the *xz* direction for which the image of gas–liquid distribution during two-phase flow is shown in (b). The data acquisition time for the image shown in (b) is 160 ms. The presence of water is indicated by high intensity (white); gas and ceramic are identified by zero intensity (black). The area within the solid white bars in (b) defines the region of analysis. Prior to calculating the bubble size and velocity distributions, the image data are binary gated to identify voxels containing either gas or liquid.

Subsequent sets of four images were acquired following a time delay of 3 s. Fig. 1a shows a 2D transverse (*xy*) ^{1}H image of a fully water-saturated monolith in the absence of flow; in-plane spatial resolution is 391 μm × 391 μm. The boxed area shows the location of the *xz* slice for which a single image frame acquired during two-phase flow is shown in Fig. 1b; in-plane pixel resolution is 391 μm (*x*) × 781 μm (*z*). The thickness of the image slice is 1.0 mm.

Inspection of Fig. 1b clearly shows that it is possible to image individual gas bubbles (zero image intensity) within the channels of the monolith. The bubble-size distribution and liquid-phase volume fraction are obtained following binary gating of the image data. The liquid-phase volume fraction obtained from Fig. 1b is 0.61 ± 0.03 which compares well with values obtained volumetrically for liquid holdups in normal co-current down-flow contactor reactor operation, typically 0.5–0.7 [22]. Bubble-size and bubble-velocity distributions, as shown in Fig. 2, are calculated from multiple image frames of the type shown in Fig. 1b. The bubble-velocity distribution shown in Fig. 2b is obtained by following the position of the gas–liquid interface characterising each bubble between successive pairs of images. It should be noted that only bubbles wholly contained within the area bounded by white lines in Fig. 1b are included in the analysis. Analysis of the data presented here confirm that the system is demonstrating bubble-train flow and that MRI can be used as a quantitative tool to probe two-phase flow within ceramic channels over timescales as short as 160 ms. Preliminary observations made from this study were that the bubble velocity was not stable with time, and that bubble motion in the direction opposite to that of the superficial flow within individual channels does occur, as expected given the possibility of negative pressure drop

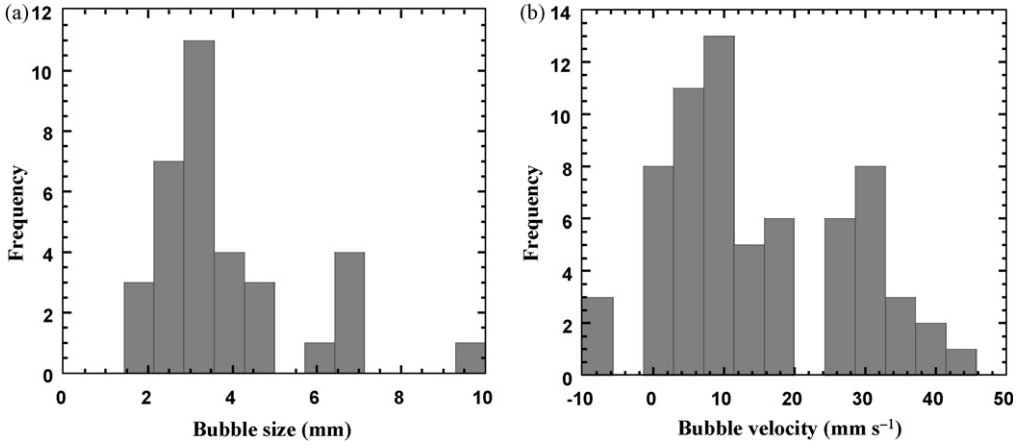

Fig. 2. (a) Bubble-size, and (b) bubble-velocity distributions obtained from series of images acquired at 160 ms time intervals, of the type shown in Fig. 1b. The bubble-size distribution is obtained directly from such an image, following gating. The distribution of bubble velocities is obtained by identifying the position of the gas–liquid interface in two successive images recorded for a single r.f. excitation.

existing at different locations across the monolith [8]. The SEMI-RARE approach was later extended to study gas-phase volume fraction and bubble-velocity distributions characterising Taylor flow during gas up-flow in stagnant water through two sets of ceramic (cordierite) monoliths, rated at 300 and 400 cpsi [23].

Despite the achievements of this early work [19,20,23], there exist a number of limitations in the application of SEMI-RARE to measuring two-phase flow in monoliths. The two most obvious arise from the fact that velocities are calculated by identifying an individual gas–liquid interface in at least two successive images. Therefore, we cannot measure liquid velocity in a pure liquid-filled channel. Further, for a given interface to be seen in two successive frames, within a field-of-view (FOV) of 5 cm, a maximum liquid velocity of only $\sim$10 cm s^{-1} can be studied. This estimate assumes that for a given FOV of 5 cm, the region of homogeneity in the static and r.f. magnetic fields required for us to track the moving interface accurately (i.e., requiring good signal-to-noise in the image) actually reduces the FOV to an effective FOV of 3.5 cm. Two further limitations exist. First, the system under study must give a coherent signal over typical timescales of $\sim$300 ms; thus fluctuations in the flow over shorter timescales than this will lead to errors in the velocity distributions obtained. Second, in channels in which fast fluid velocity exists, 'washout' may make a 'fast flow' channel appear to be associated with zero signal intensity and therefore be identified as a gas-filled channel. 'Washout' may be understood as follows. MR experiments essentially comprise an excitation pulse followed at a later time by recording of the signal. If the initially excited signal has moved out of the FOV before the signal is recorded, zero MR signal is acquired. For the type of set-ups described in Fig. 1, 'washout' will occur at $\sim$60 cm s^{-1}; this estimate is based on a FOV of 5 cm and taking the observation time to be half of the single image acquisition time; typically $\sim$90 ms.

In this paper we report the development of two new MR strategies for extending the range of applicability of MR to characterise flow in parallel channel ceramic monoliths. These MR techniques are: (i) line-excitation time-of-flight (TOF), and (ii) displacement tracking using time-resolved phase mapping; we refer to this second measurement method as the displacement tracking technique. We first describe the principles upon which these measurements are based. Initial results for co-current gas–liquid up-flow operation of a monolith rated at 200 cpsi are then reported. The principle achievement of the displacement tracking technique is that liquid velocities within both gas–liquid and completely liquid filled channels can now be quantified up to velocities of 5–10 m s^{-1}.

2. New strategies for characterising two-phase flow in monoliths

First we introduce the strategy used in the line excitation TOF experiment. As its name suggests, the new pulse sequence measures velocity based on a TOF principle, and it achieves this by combining a line excitation strategy with the SEMI-RARE pulse sequence [24]. TOF or 'spin tagging' methods were first reported in 1959 [25] and their use has been widespread since then, particularly with respect to velocity measurement. In its simplest form, the TOF approach monitors velocity by following, by analysis of successive image acquisitions, the movement of a selectively-excited population of nuclear spins within the sample. MR signal is subsequently acquired only from these initially excited spins. In the present implementation of the line excitation SEMI-RARE pulse sequence, a line of spins across the monolith is excited (in this case the 'line' is a band of spins of height 5 mm) and their movement is then followed in successive SEMI-RARE images. The second method, which we refer to as 'displacement tracking', measures displacement directly from the phase shift of the MR signal at increasing time intervals. The pulse sequence used to achieve this is again based on SEMI-RARE, and has been given the acronym COTTAGE which stands for COntinous Translational Tracking using Alternate Gradient Encoding.

The line excitation and displacement tracking techniques reported here complement and offer significant advantages in some circumstances over the standard SEMI-RARE approach described earlier. In summary, the advantages and particular characteristics of these two approaches are as follows. The Line Excitation TOF approach: (i) obtains velocity measurements from a single image; i.e. only one image acquisition is acquired reducing minimum data acquisition times to $\sim$160 ms. This increases the possible upper limit in velocity that can be studied to $\sim$20 cm s^{-1} compared to the value of 10 cm s^{-1} using the SEMI-RARE method. (ii) In a single image acquisition, the extent of flow heterogeneity (i.e. up- and down-flow) within the monolith is characterised. (iii) The liquid velocity in channels which are completely liquid-filled within the FOV at the time of measurement can be measured. (iv) The flow profile across each channel is spatially resolved. (v) The probability distribution of displacements for a given observation time within each channel can be obtained. The COTTAGE displacement tracking approach offers even greater flexibility and has the following characteristics: (i) As with line excitation, the liquid velocity in channels which are either completely liquid-filled or contain gas and liquid is measured. (ii) The potential upper limit on liquid velocity that can be studied is 5–10 m s^{-1}. This is because the velocity encoding measurement can be done in less than 3 ms using a single position-encoding gradient. (iii) Successive acquisitions allow the tracking of fluid displacement such that temporal variations in velocity, of order the data acquisition time for a single image frame (typically $\sim$3–10 ms), can be tracked for a duration of 0.5–1 s within a single experiment.

To understand the principles of the two novel MR measurements reported here, the **k**-space sampling strategies upon which the pulse sequences are based need to be understood. Acquisition of data in an MR imaging experiment can be thought of in an analogous way to that of the acquisition of data in neutron or X-ray scattering. That is, the data can be considered as being acquired in reciprocal space. For MR applications these data are referred to as **k**-space data which are then Fourier-transformed to yield real space data. Expressed formally, the **k**-space vector is defined as $\mathbf{k} = (\gamma \mathbf{G} t/2\pi)$ [26],

where γ is the gyromagnetic ratio, **G** represents the applied magnetic field gradient, and t is the time for which the magnetic field gradient is applied. The acquired MR signal (written for the general case of 3D) can be written in terms of the **k**-space vector as:

$$S(\mathbf{k}) = \iiint \rho(\mathbf{r}) \exp[\mathrm{i}2\pi\mathbf{k}\cdot\mathbf{r}]\,\mathrm{d}\mathbf{r} \quad (1)$$

where S(**k**) represents the complex data acquired, which comprises magnitude and phase information. The spatial distribution of spins is then given by the inverse 3D Fourier transform:

$$\rho(\mathbf{r}) = \iiint S(\mathbf{k}) \exp[-\mathrm{i}2\pi\gamma\mathbf{k}\cdot\mathbf{r}]\,\mathrm{d}\mathbf{k} \quad (2)$$

Thus, if we wish to acquire a 2D image in the xz plane (such as that shown in Fig. 1b, we have to acquire data that samples **k**-space in the x- and z-directions. This is achieved by applying magnetic field gradients in the x- and z- directions during the MR experiment. The basic SEMI-RARE sequence along with the **k**-space raster is shown in Fig. 3. Successive lines of **k**-space are 'read' by applying a magnetic field gradient along the x-direction (often referred to as the 'read'-direction), and identified here as G_r. The acquired data are referred to as an 'echo' (see Fig. 3a). To move up and down the **k**-space raster we have to move to different values of k_z; this is achieved by applying different magnitudes of the magnetic field gradient, G_p, along the z- (or 'phase'-) direction for a known duration. Different values of G_p (equivalently G_z) are applied in successive iterations of the pulse sequence. Therefore we see that successive lines of **k**-space are read by ramping through the values of k_z. After each line of **k**-space is read, we first move back to $k_z = 0$ by the application of an opposite polarity gradient in the phase direction and then to the left-side of the raster (so that each line of **k**-space is read from left to right) by the application of the π r.f. pulse. The effect of the line of gradient pulses identified as G_s is as follows. Gradient pulses (i) and (iii) provide slice selection so that only one row of channels is studied. Pulse (ii) acts both as a slice refocusing pulse and a homospoil gradient pulse. Pulses (iv) and (v) are both homospoil pulses. The SEMI-RARE pulse sequence is looped through $n_i \times n_p$ times to produce n_i images, each containing n_p lines of **k**-space. When $n_i = 1$, this pulse sequence reduces to the original Single Shot RARE (or Turbo Spin Echo) pulse sequence proposed by Hennig et al. [21]. To acquire the xy image shown in Fig. 1a, the G_s and G_p gradients will be switched to be applied along the z- and y-directions, respectively; i.e. we will acquire data from an xy slice with slice selection along the direction of superficial flow (z).

The line excitation SEMI-RARE pulse sequence used to acquire the line excitation TOF data is shown in Fig. 4a, where the phase gradient sequence (i) is used. The standard SEMI-RARE pulse sequence is combined with a TOF experiment by implementing SEMI-RARE such that a plane of magnetisation is excited with the excitation pulse perpendicular to the imaging slice; i.e. a line of nuclear spins is excited across the image. The excited spins which are also in the imaging plane are then tracked in subsequent image acquisitions using a conventional TOF approach. In the implementation presented here, the excitation slice is perpendicular to the imaging slice so that only a thin line of magnetisation is excited and subsequently refocused. The line excitation is achieved by the application of a gradient in the phase direction applied simultaneously with the $\pi/2$ r.f. pulse and followed by a refocusing gradient pulse.

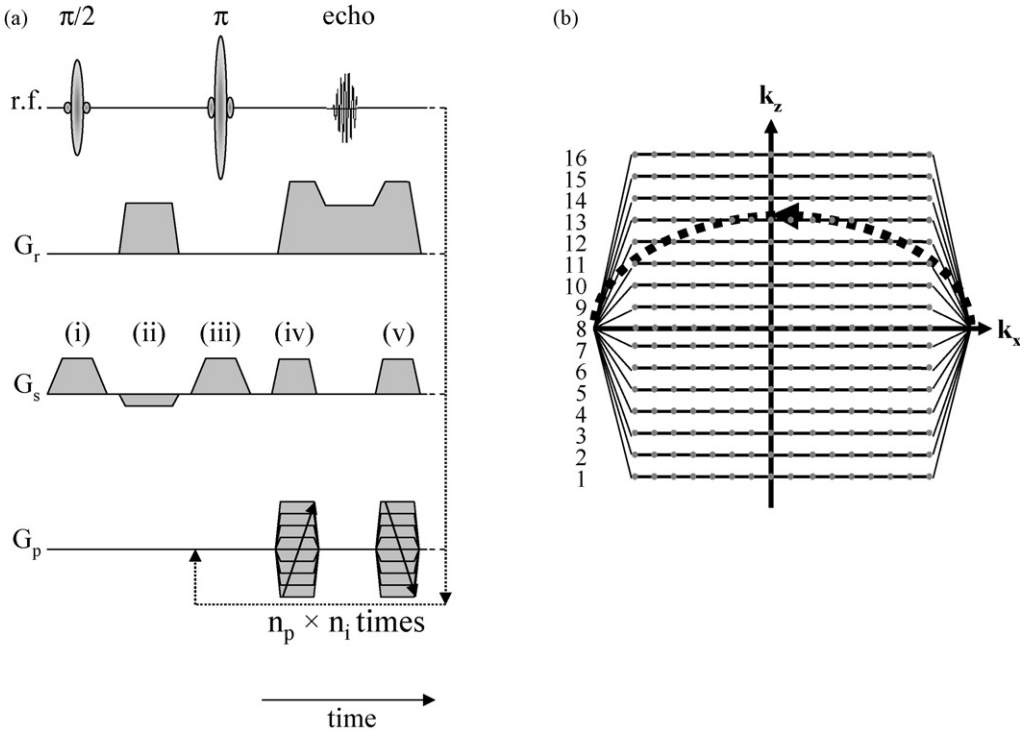

Fig. 3. (a) SEMI-RARE pulse sequence, and (b) associated **k**-space raster.

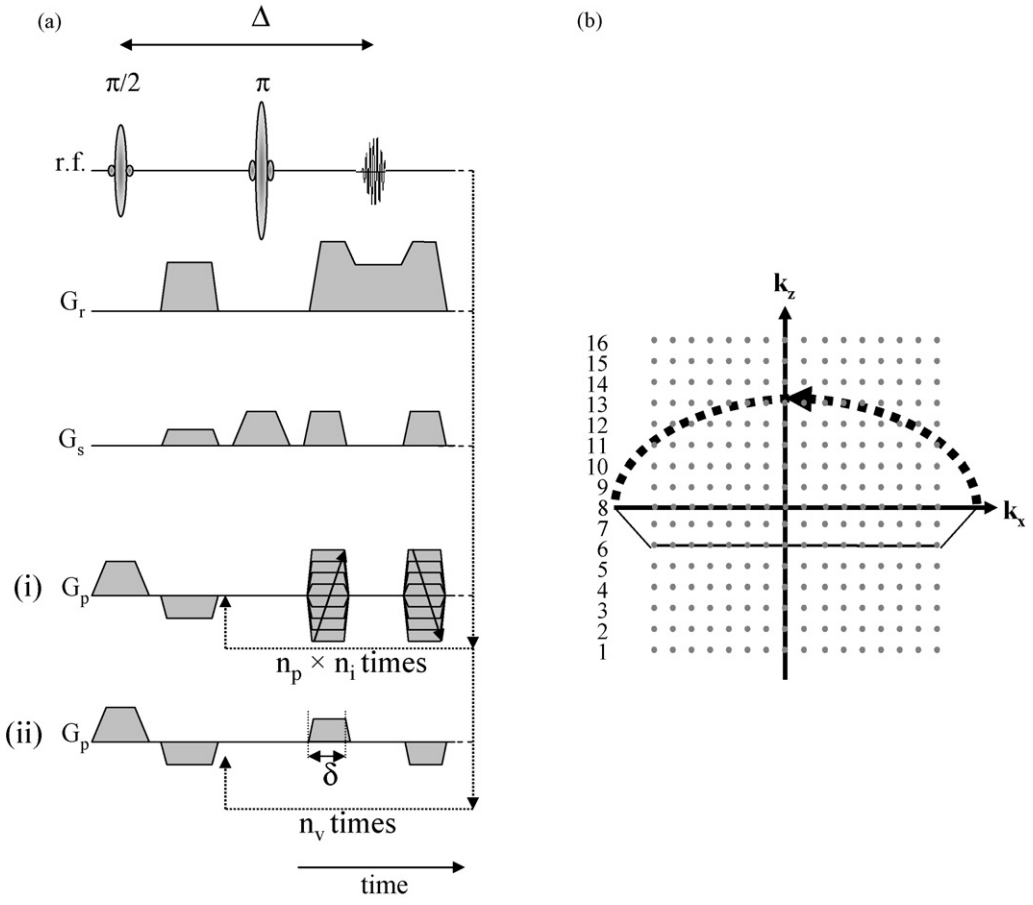

Fig. 4. (a) SEMI-RARE pulse sequence modified for (i) line excitation TOF; the line excitation SEMI-RARE pulse sequence, and (ii) the displacement tracking technique; the COTTAGE pulse sequence. (b) The **k**-space raster describing the **k**-space sampling strategy of the COTTAGE pulse sequence.

The data collected are acquired only from a single row of channels. The spatial distribution of intensity observed in the resulting images is similar to a probability distribution of displacements, i.e. a displacement propagator convolved with the initial excitation profile. It is worth noting that by acquiring successive image frames, the line excitation SEMI-RARE pulse sequence allows a greater dynamic range of liquid velocities to be studied than is possible by acquiring single velocity images using other TOF techniques since each successive image will have a different dynamic range.

The COTTAGE pulse sequence used for the displacement tracking measurement is shown in Fig. 4a with the phase gradient sequence (ii) being used. The **k**-space raster for this sequence is shown in Fig. 4b; it is seen that we acquire the same line of **k**-space during each echo in the RARE sequence. Each line, when Fourier transformed in only the *x*- (read) direction, will correspond to a projection of the system in the phase direction, and by examining the phase of the signal at each *x*-coordinate point we will obtain information on the average displacement of the fluid in the phase direction at that coordinate. The echo train will therefore give us a series of one-dimensional profiles showing the evolution of the phase angle for each echo; i.e. at increasing acquisition times. In short, we have sacrificed information on the spread of the displacement for enhanced temporal resolution. The phase data obtained in this way provides a measurement of the distance moved over the time since the initial r.f. excitation. The phase, ϕ, characterising the spin system is related to the distance, z, moved in the direction of the gradient by the spins from their position at the time of the initial r.f. excitation by the expression:

$$\phi = \gamma G_z z \delta \tag{3}$$

where δ is the time over which the magnetic field gradient applied in the z-direction (i.e. phase direction) is applied (see Fig. 4a). Once z is obtained, it is straightforward to calculate the velocity, v, with which the spins are moving since $v = z/T$; $T = n_v \Delta$ where Δ is the observation time (see Fig. 4a). The magnitude of the applied magnetic field gradients is selected subject to the magnitude of the velocities to be measured and the need to acquire data of sufficient signal-to-noise. For example, larger magnetic field gradients give greater resolution in the phase-angle measurement (this would be important when quantifying low flow velocities) but will also reduce the signal-to-noise of the acquired data. Thus for a general system we might consider taking two measurements, with both low and high gradients such that high and low velocities may be measured with similar degrees of accuracy.

3. Experimental

A flow loop consisting of a Perspex® column, of 50 mm i.d., containing a cylindrical, square-channel ceramic monolith, was positioned within the vertical bore of the magnet. The monolith was of diameter 42 mm and length 0.15 m, and rated at 200 cpsi, with each channel having a square cross-section of side 1.7 mm. The monolith was held in place with a rubber 'O'-ring and a Teflon wrapping, which ensured that no fluid bypassed the monolith at the sides.

The flow rig was operated under conditions of co-current gas-liquid up-flow. The gas up-flow was implemented by introducing compressed air to the base of the liquid-flooded unit, through a glass sintered frit of diameter 20 mm at a vertical distance of 59 cm from the base of the monolith, in a similar configuration to that reported previously in Sederman et al. [23]. The gas used was air. The liquid used was water to which 3 wt% of propan-2-ol had been added to reduce the liquid–gas surface tension such that the bubbles produced at the glass frit would easily enter the monolith channels. The liquid was pumped using a Verdergear VG330-10 gear pump, and the flow rate was measured using a Bronkhorst coriolis mass flow controller (model M55C4-AAD-11-K-C), measuring to an accuracy of ±1.0%. The gas flow rate was measured with a GPE rotameter (model number 10311); typical errors in gas flow rates are ±5%. Data are reported here for the monolith operating under conditions of a constant gas flow rate of 100 $cm^3\ min^{-1}$ (0.9 $mm\ s^{-1}$), at liquid flow rates of 29, 78 and 105 $l\ h^{-1}$, corresponding to 4.1, 11.0 and 14.9 $mm\ s^{-1}$, respectively.

MRI experiments were carried out on a Bruker Spectrospin DMX 200, 4.7 T magnet with a birdcage coil of length and diameter 6.3 cm. Proton (^1H) images were acquired at a frequency of 199.7 MHz. Spatial resolution was achieved using shielded gradient coils providing a maximum gradient strength of 13.9 $G\ cm^{-1}$.

In the case of the line excitation SEMI-RARE pulse sequence, four images were acquired after each excitation with each image having a data acquisition time of 182 ms. Effective image times are taken as 91, 274, 456 and 638 ms after the initial excitation. The images consist of a 128 (x-read) ×64 (z-phase) data array with FOV of 51 mm × 35 mm and in-plane spatial resolution of 398 μm × 547 μm. The initial excitation of the 'line' of spins over a height 5 mm in the phase (z) direction was achieved using a sinc-shaped soft pulse truncated at three lobes, of duration 512 μs. The soft π pulse acts as both a refocusing pulse and the slice selection pulse in the y-direction. In this case a slice of thickness 1.7 mm was used; the refocusing pulse was also of duration 512 μs and sinc-shape, truncated at three lobes. This slice thickness and excitation shape was chosen to ensure that the excited fluid existed within the single row of channels of interest. The direction of superficial flow was chosen to be in the phase direction so as to minimise flow artefacts in the images, and the read gradient was chosen to be in the x- direction since the read direction is not flow-compensated. The echo time, Δ, was 2.85 ms. The recycle time was 10 s. A line excitation TOF dataset was acquired under conditions of zero flow (i.e. with a fully liquid-filled monolith) and this was used as a reference dataset for all datasets acquired under flowing conditions.

Implementation of the displacement tracking measurement was the same as that used for line excitation, except that the magnetic field gradients in the phase direction were applied according to scheme (ii) in Fig. 4a, as opposed to scheme (i). The duration, δ, of the de-phasing gradient was 380 μs. The pulse sequence is looped n_v times; in this case $n_v = 256$, thereby producing 256 velocity measurements spaced at integer values of Δ. The delay Δ, will typically be ∼3 ms. A time-resolved phase map was acquired under conditions of zero flow (i.e. with a fully liquid-filled monolith) and this was used as a reference dataset for all datasets acquired under flowing conditions.

4. Results and discussion

A typical line excitation TOF dataset is shown in Fig. 5a. Significant liquid displacement is only seen in the direction of superficial flow as expected given the operating conditions of co-current gas–liquid up-flow. The heterogeneity in the flow is clearly seen. In several channels very little displacement has occurred over the 182 ms observation time. For example, in channel number 3 the distribution in intensity appears to be symmetrical about a displacement of zero, suggesting that the water is stagnant within this channel, the only displacement process being molecular diffusion. In contrast, in channel 20 there is fast liquid flow and a displacement profile across the width of the channel is clearly seen. Channel 15 shows no evidence of signal intensity, and therefore must have been gas filled over the 5 mm height of the initial line excitation.

The analysis of line excitation TOF data proceeded as follows. The images recorded in all cases were taken in the xz-plane, where z is the direction of superficial flow (i.e. along the axial direction of the monolith channels). First, the ceramic walls of the monolith were identified in the reference image taken of the liquid-saturated monolith. A mask was created by binary gating this reference image following identification of local minima in the signal intensity which were associated with the channel walls of the monolith. Having applied the reference mask to the line excitation image, the remaining signal intensity was then assigned to be associated with liquid within the monolith. The velocity distribution of liquid within the monolith channels was obtained from these data by averaging in the x-direction such that a single value of signal intensity was acquired for each channel at every point in the z-direction. The position of the maximum in the signal intensity along the length of each channel was then identified following boxcar smoothing of the intensity data to reduce errors arising from noise in the data. The z-position of the maximum in signal intensity was taken as the value of displacement used in the calculation of velocity. For each image (such as that shown in Fig. 5a), data from 26 channels were analysed. Velocity distributions were calculated from data obtained from 64 repetitions of the pulse sequence; i.e. 64 datasets such as that shown in Fig. 5a. In principle, the liquid phase holdup can be estimated from these data. The magnitude of the signal

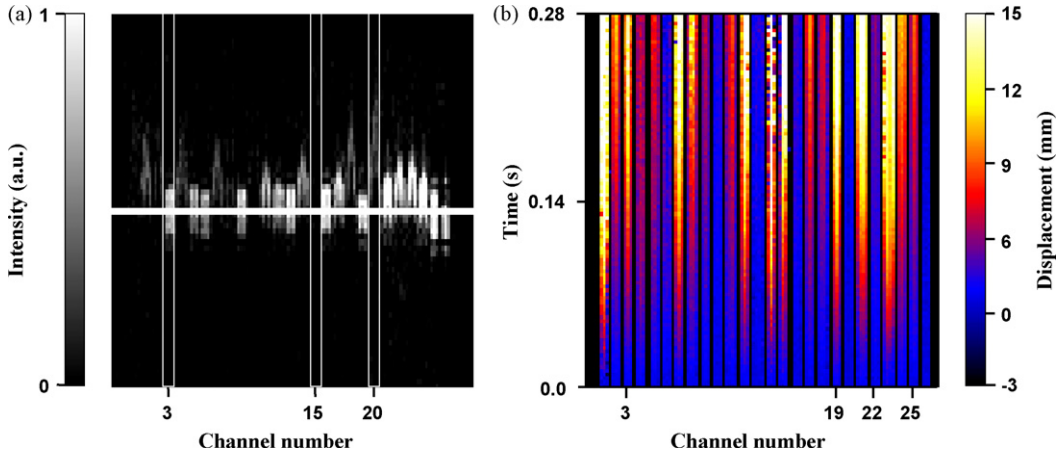

Fig. 5. Data acquired using (a) line excitation TOF, and (b) displacement tracking techniques. Particular channels referred to in the text are identified in the figure. The air and liquid superficial velocities were 0.9 and 11.0 mm s^{-1}, respectively, in both experiments. In (a), the signal intensity shows the position of liquid within each channel at a time 91 ms after the initial excitation. Faster liquid velocities will tend to correspond to lower signal intensities because the water is distributed along a greater distance within the channel. The horizontal white line corresponds to the central (zero displacement) position and the FOV in the flow direction is 35 mm. The vertical white lines identify the channels discussed in the text. (b) The displacement tracking technique measures displacement as a function of both time and position across the channel.

intensity seen within each channel will be attenuated, to some degree, at high liquid velocity, therefore direct integration of the signal intensity will not provide an accurate measure of holdup. However, use of a binary gating method [19,23] to identify liquid-containing pixels will provide a measure of the fraction of the number of pixels, initially excited in the 5 mm slice, that contained liquid; i.e. the holdup. In practice, data from multiple excitations should be acquired to provide an estimate of holdup that is representative of the flow within the monolith.

A typical displacement tracking dataset is shown in Fig. 5b. The colour scale corresponds to the displacement of the fluid, within each channel, over a range of observation times ranging from 0.003 to 0.28 s. From this map, the time-variation of liquid velocity within each channel may be plotted. Two ways of plotting these results are shown in Figs. 6 and 7, respectively. In Fig. 6, displacement versus time plots are shown for four channels (the channels are indicated in Fig. 5b). To produce the analysed data, as with the line excitation data, the walls of the monolith are identified and removed from the analysis using the reference map. The value of phase, and hence displacement is then averaged across each channel. It is worth noting that while flow velocity remains constant in the four channels shown in Fig. 6, flow reversal and change in velocity over timescales of 50–100 ms has been observed under some operating conditions. In Fig. 7, the displacement profile along each channel is plotted for two observation times: 140 and 280 ms. To produce the data shown in Fig. 7, the data are not averaged along the *x*-direction

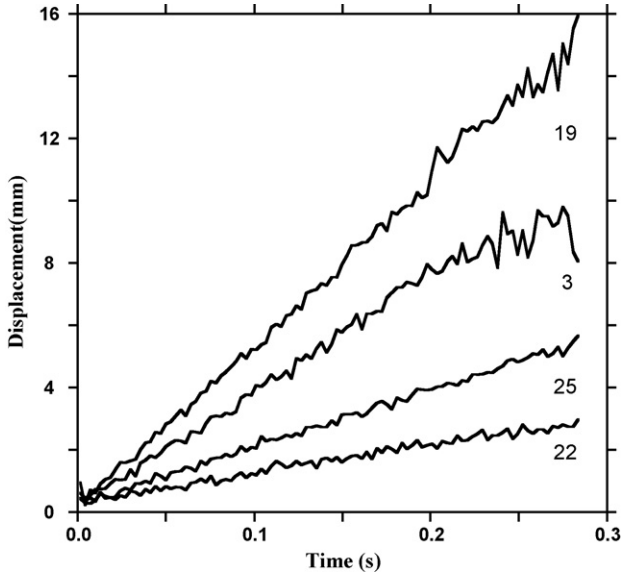

Fig. 6. Analysis of displacement tracking data shown in Fig. 5b. The plots show the mean fluid displacement as a function of time for four channels (identified on Fig. 5b).

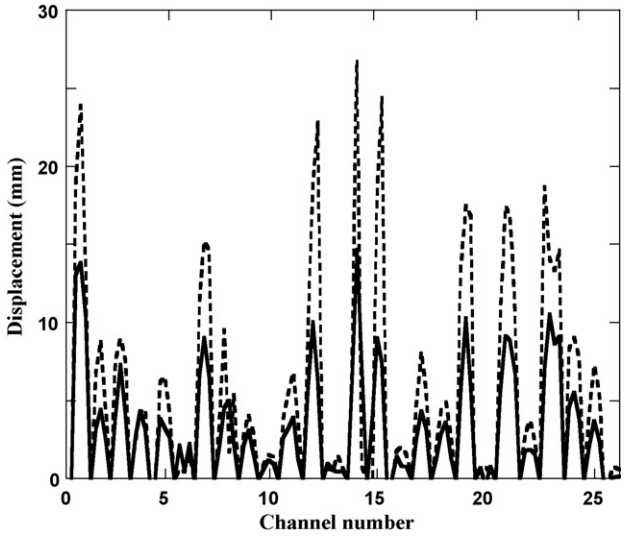

Fig. 7. Profiles of liquid displacement within each channel obtained using the displacement tracking technique. Profiles are shown for observation times of 140 ms (—) and 280 ms (- - - -).

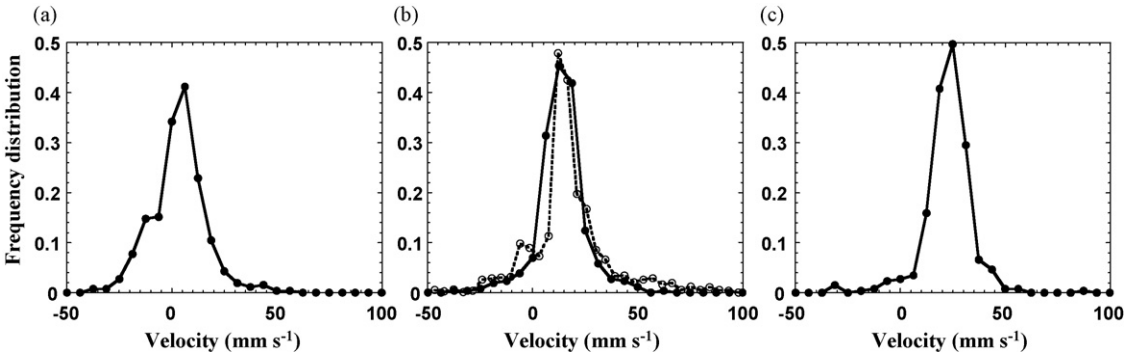

Fig. 8. Velocity histograms calculated from the displacement tracking measurements (—). The monolith was operating under conditions of co-current gas–liquid up-flow, with a constant superficial gas velocity of 0.9 mm s^{-1} and superficial liquid velocities of (a) 4.1, (b) 11.0 and (c) 14.9 mm s^{-1}, respectively. In (b) the data obtained from a line excitation TOF experiment are also shown.

within an individual channel, hence displacement profiles within each channel are obtained. Fig. 8 shows the liquid velocity histograms recorded using the displacement tracking technique. The velocities which make up the histograms are calculated from the gradient of the first 20 data points (57 ms) forming each of the four lines shown in Fig. 6 and for all other channels in the slice. Data from 16 experiments are used to derive the histograms shown in Fig. 8. Results are shown for experiments recorded using the displacement tracking technique with a constant gas flow rate of 0.9 mm s^{-1} and liquid flow velocities of 4.1, 11.0 and 14.9 mm s^{-1}, the mean and standard deviation (written as mean:standard deviation) of the velocity histograms for each of these velocities are (3.2:10.4), (13.6:9.2) and (22.5:8.8), respectively. We see that the spread in the distribution of liquid velocities within the monolith decreases as liquid velocity through the monolith increases. Further, particularly at low velocities, there exists substantial up-flow and down-flow within the monolith consistent with the results of Thulasidas et al. [27] who proposed that significant backmixing occurs under these conditions. In Fig. 8b, the data obtained using the line excitation TOF approach is compared with that obtained by displacement tracking. The mean and standard deviation values calculated from the line excitation TOF and displacement tracking data are (16.1:12.1) and (13.6:9.2), respectively, showing good agreement. This is particularly reassuring since the two measurements are based on quite different principles. In the case of line excitation TOF we are measuring displacement directly—by following the movement of a specific population of initially excited spins. In contrast, the displacement tracking technique measures the phase of the received MR signal as a function of time, from which displacement as a function of time is calculated. It is also important to note that in this paper we are reporting the development of these techniques and demonstrating their use. In applying these methods in a systematic study of two-phase flow in channels, it will be important to design the data acquisition such that data are acquired from several cross-sections along the length of the monolith, as well as several acquisitions being made at each vertical position; i.e., it is important to acquire data that are representative of the whole monolith. When comparing the mean superficial velocities in Fig. 8 with the superficial velocities characterising the feed, we also note that the feed superficial velocity has been based on the column diameter, and no allowance has been made for the reduced cross-sectional area arising from the walls of the monolith. Also since we have only collected data from one cross section within the monolith, we will not have fully sampled the flow within the monolith to account for, for example, any flow misdistributions at the inlet.

The development of the line excitation TOF and displacement tracking techniques significantly extend our ability to quantify hydrodynamics in parallel channel ceramic monoliths. Both these new techniques may be used in combination with our original SEMI-RARE pulse sequence [19,20] which acquires 2D images of the gas and liquid distribution within the monolith on timescales of ∼100 ms. The line excitation TOF method allows slightly higher liquid velocities to be measured than was possible with the standard SEMI-RARE pulse sequence, and has the advantage that the heterogeneity of the flow characteristics within the monolith are characterised within a single image acquisition (Fig. 5a) which takes ∼100–200 ms to acquire. The displacement tracking technique has a significantly greater dynamic range in velocity measurement compared to the other two approaches and, since it is a faster measurement (∼3–10 ms), also allows us to measure liquid movement within individual channels as a function of time. Typically 100 repetitions of the pulse sequence can be made in immediate succession thereby allowing us to track displacement over timescales of ∼1 s.

5. Conclusion

Two new MR pulse sequences are reported which significantly increase the ability of MR to measure two-phase flow in ceramic monoliths. The SEMI-RARE pulse sequence previously reported is able to image the gas and liquid distribution along a channel but is unable to image liquid velocity in a liquid-filled channel, and cannot measure liquid slug/bubble velocities greater than ∼10 cm s^{-1}. The new pulse sequences sacrifice information on the gas–liquid distribution along the length of individual channels, but significantly increase the range of liquid velocities that can be studied such

that MR can now be applied to operating conditions of industrial interest. Further, both the line excitation TOF and displacement tracking techniques give quantitative data on liquid velocities in both gas–liquid and completely liquid-filled channels. Whilst the line-excitation approach cannot measure liquid velocities greater than $\sim$20 cm s^{-1}, the displacement tracking technique has an upper limit of 5–10 m s^{-1}. The displacement tracking technique also enables us to measure fluid displacement within individual channels with a time resolution of $\sim$10 ms, thereby enabling us to study, in real-time, the stability of the flow within the monolith.

Acknowledgements

We thank EPSRC for financial support of this work (GR/S20789/01). We also thank Dr. P. Alexander for his help in the preparation of this manuscript.

References

[1] C. Boyer, A.-M. Duquenne, G. Wild, Chem. Eng. Sci. 57 (2002) 3185.
[2] L.F. Gladden, M.D. Mantle, A.J. Sederman, Adv. Catal. 50 (2006) 1.
[3] S. Irandoust, B. Andersson, Catal. Rev. Sci. Eng. 30 (1988) 341.
[4] S. Irandoust, B. Andersson, Chem. Eng. Sci. 43 (1988) 1983.
[5] S. Irandoust, A. Cybulski, J.A. Moulijn, The use of monolithic catalysts for three phase reaction, in: A. Cybulski, J.A. Moulijn (Eds.), Structured Catalysts and Reactors, Marcel Dekker, New York, 1998, p. 239.
[6] T.A. Nijhuis, M.T. Kreutzer, A.C.J. Romijn, F. Kapteijn, J.A. Moulijn, Chem. Eng. Sci. 56 (2001) 823.
[7] M.T. Kreutzer, J.J.W. Bakker, F. Kapteijn, J.A. Moulijn, P.J.T. Verheijen, Ind. Eng. Chem. Res. 44 (2005) 4898.
[8] D. Mewes, T. Loser, M. Millies, Chem. Eng. Sci. 54 (1999) 4729.
[9] T. Bauer, S. Roy, R. Lange, M. Al-Dahhan, Chem. Eng. Sci. 60 (2005) 3101.
[10] T. Kraus, A. Günther, N. Mas, M.A. Schmidt, K.F. Jensen, Exp. Fluids 36 (2004) 819.
[11] E.H.L. Yuen, A.J. Sederman, L.F. Gladden, Appl. Catal. A232 (2002) 29.
[12] I.V. Koptyug, A.A. Lysova, A. Kulikov, V.A. Kirillov, V.N. Parmon, R.Z. Sagdeev, Appl. Catal. A267 (2004) 143.
[13] B.S. Akpa, M.D. Mantle, A.J. Sederman, L.F. Gladden, J. Chem. Soc., Chem. Commun. (2005) 2741.
[14] A.J. Sederman, M.D. Mantle, C.P. Dunckley, Z.Y. Huang, L.F. Gladden, Catal. Lett. 103 (2005) 1.
[15] I.V. Koptyug, S.A. Altobelli, E. Fukushima, A.V. Matveev, R.Z. Sagdeev, J. Magn. Reson. 147 (2000) 36.
[16] I.V. Koptyug, L.Y. Ilyina, A.V. Matveev, R.Z. Sagdeev, V.N. Parmon, S.A. Altobelli, Catal. Today 69 (2001) 385.
[17] A.K. Heibel, T.W.J. Scheenen, J.J. Heiszwolf, H. Van As, F. Kapteijn, J.A. Moulijn, Chem. Eng. Sci. 56 (2001) 5935.
[18] A.K. Heibel, F.J. Vergeldt, H. Van As, AIChE J. 49 (2003) 3007.
[19] M.D. Mantle, A.J. Sederman, L.F. Gladden, S. Raymahasay, J.M. Winterbottom, E.H. Stitt, AIChE J. 48 (2002) 909.
[20] A.J. Sederman, M.D. Mantle, L.F. Gladden, J. Magn. Reson. 161 (2003) 15.
[21] J. Hennig, A. Nauerth, H. Friedburg, Magn. Reson. Med. 3 (1986) 823.
[22] A.P. Boyes, A. Chughtai, X.X. Lu, S. Raymahasay, S. Sarmento, M.W. Tilston, J.M. Winterbottom, Chem. Eng. Sci. 47 (1992) 3729.
[23] A.J. Sederman, M.D. Mantle, L.F. Gladden, Magn. Reson. Imaging 21 (2003) 359.
[24] J.J. Heras, A.J. Sederman, L.F. Gladden, Magn. Reson. Imaging 23 (2005) 387.
[25] J.R. Singer, Science 30 (1959) 1652.
[26] P. Mansfield, P.K. Grannell, J. Phys. C. 6 (1973) L422.
[27] T.C. Thulasidas, M.A. Abraham, R.L. Cerro, Chem. Eng. Sci. 54 (1999) 61.